Science Advances
AAAS

Supplementary Materials for

Field theory spin and momentum in water waves

Konstantin Y. Bliokh*, Horst Punzmann, Hua Xia, Franco Nori, Michael Shats*

*Corresponding author. Email: k.bliokh@gmail.com (K.Y.B.); michaelshat@gmail.com (M.S.)

Published 21 January 2022, *Sci. Adv.* **8**, eabm1295 (2022)
DOI: 10.1126/sciadv.abm1295

This PDF file includes:

Sections S1 to S3
Figs. S1 and S2
References

1. Theoretical calculations

1.1. Equations of motion for gravity waves

We first derive the main wave equation describing the motion of water particles in deep-water gravity waves. We consider linear waves on the surface of an incompressible fluid (water). The fluid motion can be described by the Eulerian 3D velocity field $\mathbf{v}(\mathbf{r},t)$ and the velocity potential $\phi(\mathbf{r},t)$: $\mathbf{v} = \nabla\phi$. Denoting the 2D in-plane velocity components and gradient via $\mathbf{V} = (v_x, v_y)$ and $\nabla_2 = (\partial_x, \partial_y)$, as well as the normal velocity component $W = v_z$, the equations of motion can be written as [31,54]:

$$\partial_t^2\phi = -g\partial_z\phi \quad \text{for} \quad z = 0, \quad \nabla^2\phi = \nabla\cdot\mathbf{v} = \nabla_2\cdot\mathbf{V} + \partial_z W = 0, \tag{S1}$$

where g is the gravitational acceleration.

Applying the operator ∇_2 to the first equation (S1) and using $W = \partial_z\phi$, we obtain

$$\partial_t^2\mathbf{V} = -g\nabla_2 W \quad \text{for} \quad z = 0. \tag{S2}$$

Because of the linear character of gravity waves and proportionality of all the scalar wave fields in deep-water surface waves, we can write the first Eq. (S1) as $\partial_t^2 W = -g\partial_z W$ for $z = 0$. Using the second Eq. (S1), we derive

$$\partial_t^2 W = g\nabla_2\cdot\mathbf{V} \quad \text{for} \quad z = 0. \tag{S3}$$

Equations (S2) and (S3) are the desired wave equations for the velocity field at the water surface. Monochromatic waves with a fixed frequency ω can be described by complex wave amplitudes introduced via $\{\mathbf{v}(\mathbf{r},t), \mathbf{V}(\mathbf{r},t), W(\mathbf{r},t)\} = \mathrm{Re}\left[\{\mathbf{v}(\mathbf{r}), \mathbf{V}(\mathbf{r}), W(\mathbf{r})\}e^{-i\omega t}\right]$. In this case, Eqs. (S2) and (S3) are reduced to

$$\omega^2\mathbf{V} = g\nabla_2 W, \quad \omega^2 W = -g\nabla_2\cdot\mathbf{V}. \tag{S4}$$

For a single plane wave, where all fields are proportional to $\exp(i\mathbf{k}\cdot\mathbf{r}_2)$, $\mathbf{r}_2 = (x, y)$, these equations produce the deep-water dispersion relation $\omega^2 = gk$ [31,54]. Furthermore, the relation $\omega^2 W = -ig\mathbf{k}\cdot\mathbf{V}$ in this case describes the circular motion of water particles in the propagation plane formed by the wavevector $\mathbf{k}$ and the z-axis [54]. This property is entirely analogous to the circular polarization and transverse spin of surface electromagnetic and acoustic waves [17,20–22,25,30,55,56].

While Eqs. (S2)–(S4) describe the velocity fields at the water surface, their z-dependences deep into the water can be found from the second Eq. (S1). For monochromatic waves, it follows from there that

$$\left\{ \mathbf{v}(\mathbf{r}), \mathbf{V}(\mathbf{r}), W(\mathbf{r}) \right\} = \left\{ \mathbf{v}(\mathbf{r}_2), \mathbf{V}(\mathbf{r}_2), W(\mathbf{r}_2) \right\} \exp(kz), \tag{S5}$$

where the argument $\mathbf{r}_2$ indicates that the field is taken at the water surface $z = 0$. Therefore, plane gravity waves can be regarded as *evanescent* waves with the complex 3D wavevector $\tilde{\mathbf{k}} = \mathbf{k} - ik\bar{\mathbf{z}}$ [17,30,55,56].

1.2. Analogy with sound waves

The equations of motion (S2)–(S4) look somewhat similar to the equations for sound waves in a fluid or gas [31,26,28]:

$$\beta \partial_t p = -\nabla \cdot \mathbf{v}, \qquad \rho \partial_t \mathbf{v} = -\nabla p, \tag{S6}$$

or, for monochromatic waves and the corresponding complex fields,

$$i\omega\beta p = \nabla \cdot \mathbf{v}, \qquad i\omega\rho \mathbf{v} = \nabla p. \tag{S7}$$

Here β and ρ are the compressibility and density of the medium, $\mathbf{v}(\mathbf{r},t)$ is the 3D velocity field, and $p(\mathbf{r},t)$ is the scalar pressure field.

While the similarity is obvious, there are some important differences. First, the presence of first time derivatives in the acoustic equations provides for the linear dispersion $\omega = kc_s \equiv k / \sqrt{\beta\rho}$. Second, the sound-wave equations (S6) and (S7) contain a 3D vector velocity field and a scalar pressure field, whereas the gravity-wave equations (S2)–(S4) contain a 2D velocity field and an additional scalar vertical-velocity field. Therefore, the gravity-wave equations can be associated with acoustic equations in a *2D space*. Finally, sound waves are propagating bulk modes, while gravity waves can be regarded as surface-evanescent waves exponentially decaying deep into the water.

1.3. Spin angular momentum in acoustic and gravity waves

In acoustic and water waves, the medium particles can follow complex trajectories around their unperturbed positions. The local angular momentum density associated with this motion can be written as $\rho \mathbf{a} \times \mathbf{v}$, where $\mathbf{a}$ is the displacement of the particle, such that $\mathbf{v} = \partial_t \mathbf{a}$. For monochromatic waves and complex field amplitudes, $\mathbf{v} = -i\omega\mathbf{a}$, and the time-averaged density of the angular momentum becomes

$$\rho \langle \mathbf{a} \times \mathbf{v} \rangle = \frac{\rho}{2\omega} \operatorname{Im}\left(\mathbf{v}^* \times \mathbf{v} \right), \tag{S8}$$

where $\langle ... \rangle = \frac{1}{T} \int_0^T ... \, dt$ is the time average over the oscillation period $T = 2\pi / \omega$.

For sound waves, the quantity (S8) is the acoustic *spin density* [23,25–28,56], see Table I. For gravity water waves, the angular momentum density (S8) has both the in-plane components involving the vertical velocity component $W = v_z$ and the normal component generated by the particle motion in the (x, y) plane. Since here we consider the 2D evolution of water waves and particles, we consider only the normal spin component, see Table I:

$$\mathbf{S} = \frac{\rho}{2\omega} \mathrm{Im}\left(\mathbf{V}^* \times \mathbf{V}\right). \tag{S9}$$

It should be emphasized that although the angular momentum (S8) and (S9) is produced by the microscopic *orbital* motion of the medium particles, it is associated with the *spin* angular momentum of the wave. Indeed, the orbital angular momentum of the wave is produced by the phase gradients and vortex-like macroscopic momentum flows (such as, e.g., in Fig. 3), while the spin angular momentum is generated by the rotation of the vector wave field at the given point $\mathbf{r}$ [16–21,25–28]. The latter is the case for Eqs. (S8) and (S9). Although the microscopic particle motion has a finite spatial extent, it is much smaller than the wavelength and can be made arbitrarily small by reducing the wave amplitude. The spin density normalized by the energy density is independent of this amplitude.

1.4. Stokes drift and momentum in acoustic and gravity waves

The linearized oscillatory motion of the medium particles is periodic and corresponds to closed elliptical trajectories in the monochromatic case. However, in the second-order in the wave amplitude, the medium particles can experience a slow translational motion known as the *Stokes drift* [36–38].

This phenomenon is caused by the difference between the Lagrangian and Eulerian velocities of the medium particles. So far, we have considered only the Eulerian velocity attached to a fixed spatial point $\mathbf{r}$. In the Lagrangian description, one follows a chosen particle with the Lagrangian coordinates $\boldsymbol{\xi} = \mathbf{r} + \int \mathsf{v}\, dt$. The corresponding Lagrangian velocity of the particle is $\mathsf{v}\left(\boldsymbol{\xi}, t\right)$. The time-averaged difference between the Lagrangian and Eulerian velocities provides the Stokes drift velocity:

$$\mathbf{u} = \left\langle \mathsf{v}\left(\boldsymbol{\xi}, t\right) - \mathsf{v}\left(\mathbf{r}, t\right) \right\rangle \simeq \left\langle \left[\left(\boldsymbol{\xi} - \mathbf{r}\right) \cdot \nabla\right] \mathsf{v}\left(\mathbf{r}, t\right) \right\rangle = \left\langle \left[\int \mathsf{v}\, dt \cdot \nabla\right] \mathsf{v} \right\rangle. \tag{S10}$$

For monochromatic waves, this yields

$$\mathbf{u} = \frac{1}{2\omega} \mathrm{Im}\left[\left(\mathbf{v}^* \cdot \nabla\right) \mathbf{v}\right]. \tag{S11}$$

For sound waves, Eqs. (S6) and (S7), $\nabla \times \mathbf{v} = \mathbf{0}$, and the Stokes drift (S11) can be written as

$$\mathbf{u} = \frac{1}{2\omega} \mathrm{Im}\left[\mathbf{v}^* \cdot \left(\nabla\right) \mathbf{v}\right], \tag{S12}$$

where $\left[\mathbf{v}^* \cdot \left(\nabla\right) \mathbf{v}\right]_i \equiv \sum_{j=x,y,z} v_j^* \nabla_i v_j$ [29]. Remarkably, when multiplied by the mass density ρ, the Stokes drift (S12) yields the *canonical momentum density* of sound waves: $\mathbf{P} = \rho\, \mathbf{u}$, see Table I [25,28]. To the best of our knowledge, this fact has never been noticed before. It provides a rigorous physical derivation of the canonical momentum density. Substituting the acoustic spin density (S8) and canonical momentum density into the Belinfante-Rosenfeld relation (1), and using the equations of motion (S6) and (S7), we obtain the kinetic momentum density $\mathbf{\Pi} = \frac{\beta\rho}{2} \mathrm{Re}\left(p^* \mathbf{v}\right)$ known from textbooks [31]. We emphasize that so far it was derived from the acoustic analogue of the Poynting theorem, i.e., formal mathematical analysis of macroscopic equations of motion. In contrast, here we derive all momentum and spin properties from rigorous microscopic calculations of the mechanical momentum and angular momentum of the medium particles, supplied by the fundamental field-theory relation (1). This sheds light onto the longstanding problem of the wave momentum in acoustics [43,46,51,52].

For quasi-2D gravity waves, we consider the in-plane Stokes drift and separate the contributions of the in-plane and normal velocity components into Eq. (S11):

$$\mathbf{u} = \frac{1}{2\omega}\,\mathrm{Im}\left[\left(\mathbf{V}^* \cdot \boldsymbol{\nabla}_2\right)\mathbf{V}\right] + \frac{1}{2\omega}\,\mathrm{Im}\left[W^* \partial_z \mathbf{V}\right]. \tag{S13}$$

From the first Eq. (S4) and Eq. (S5), we find that $\boldsymbol{\nabla}_2 \times \mathbf{V} = \mathbf{0}$, and $\partial_z \mathbf{V} = k\mathbf{V} = \dfrac{\omega^2}{g}\mathbf{V} = \boldsymbol{\nabla}_2 W$. As a result, Eq. (S13) can be transformed into

$$\mathbf{u} = \frac{1}{2\omega}\,\mathrm{Im}\left[\mathbf{V}^* \cdot \left(\boldsymbol{\nabla}_2\right)\mathbf{V} + W^* \boldsymbol{\nabla}_2 W\right]. \tag{S14}$$

Multiplied by the mass density, this equation provides exactly the *canonical momentum density* for gravity waves: $\mathbf{P} = \rho\,\mathbf{u}$, see Table I.

Substituting the spin density (S9) and canonical momentum density into the Belinfante-Rosenfeld relation (1), and using the equations of motion (S4), we obtain the kinetic momentum density for gravity water waves, see Table I:

$$\boldsymbol{\Pi} = \frac{\rho k}{\omega}\,\mathrm{Im}\left(W^* \mathbf{V}\right). \tag{S15}$$

Notably, this momentum density is equivalent to the conserved momentum density derived by Peskin [46]. Peskin presented it in the form $\rho \mathsf{Z}\left(\mathbf{r}_2,t\right)\mathsf{V}\left(\mathbf{r}_2,t\right)$. Here Z is the local z-elevation of the water surface, which is related to the vertical velocity as $\mathsf{W} = \partial_t \mathsf{Z}$. Performing the time averaging of this quantity for monochromatic fields and using $W = -i\omega Z$, we obtain the Peskin momentum in the form $\dfrac{\rho}{2\omega}\mathrm{Im}\left[W^*\left(\mathbf{r}_2\right)\mathbf{V}\left(\mathbf{r}_2\right)\right]$. This expression differs from Eq. (S15) by the factor of $2k$, because it represents the 2D momentum density, i.e., $\int_{-\infty}^{0} \boldsymbol{\Pi}\left(\mathbf{r}\right)dz = \dfrac{1}{2k}\boldsymbol{\Pi}\left(\mathbf{r}_2\right)$.

Note that Peskin also derived a conserved energy density of water waves, which can be written as $\dfrac{1}{2}\rho g \mathsf{Z}^2\left(\mathbf{r}_2,t\right) + \dfrac{1}{2}\rho \int_{-\infty}^{0}\left[\mathsf{V}^2\left(\mathbf{r},t\right) + \mathsf{W}^2\left(\mathbf{r},t\right)\right]dz$ [46]. Using the relations $W = -i\omega Z$ and $\int_{-\infty}^{0} \ldots dz = \left(2k\right)^{-1}\ldots$ for monochromatic fields, performing the time averaging, and multiplying the Peskin 2D energy density by $2k$ similarly to the momentum density above, we obtain the energy density for monochromatic water waves listed in Table I:

$$U = \frac{\rho}{4}\left(3\left|W\right|^2 + \left|\mathbf{V}\right|^2\right). \tag{S16}$$

This expression differs considerably from the energy density of sound or electromagnetic waves, see Table I.

Thus, the spin and canonical momentum densities introduced in this work are directly observable quantities derived from mechanical properties of water particles, which agree with the previously known kinetic wave momentum and the Belinfante-Rosenfeld relation.

1.5. Example I: Interference of two propagating gravity waves

We now consider an explicit example of an inhomogeneous gravity-wave field with nonzero momentum and spin densities. It is provided by the superposition of two plane waves of the same frequency and amplitude but orthogonal wavevectors $\mathbf{k}_1 = \frac{k}{\sqrt{2}}\left(\bar{\mathbf{x}}+\bar{\mathbf{y}}\right)$ and $\mathbf{k}_2 = \frac{k}{\sqrt{2}}\left(-\bar{\mathbf{x}}+\bar{\mathbf{y}}\right)$, where the overbars denote the unit vectors of the corresponding axes, Fig. 1. The complex velocity wave field for this superposition can be written as

$$W = A\left[e^{ik(y+x)/\sqrt{2}} + e^{ik(y-x)/\sqrt{2}}\right] = 2Ae^{iky/\sqrt{2}}\cos\left(kx/\sqrt{2}\right),$$

$$\mathbf{V} = k^{-1}\nabla_2 W = \sqrt{2}Ae^{iky/\sqrt{2}}\left[-\sin\left(kx/\sqrt{2}\right)\bar{\mathbf{x}} + i\cos\left(kx/\sqrt{2}\right)\bar{\mathbf{y}}\right], \tag{S17}$$

where A is a constant amplitude, and we consider the wavefields at the water surface $z=0$.

Substituting Eqs. (S17) into Eq. (S9), we obtain the spin density:

$$\mathbf{S} = -\frac{\rho A^2}{\omega}\sin\tilde{x}\,\bar{\mathbf{z}}, \tag{S18}$$

where $\tilde{x} = \sqrt{2}kx$. In turn, Eq. (S14) for the fields (S17) yields the canonical momentum density:

$$\mathbf{P} = \frac{\rho A^2}{\omega}\frac{k}{\sqrt{2}}\left(2+\cos\tilde{x}\right)\bar{\mathbf{y}}. \tag{S19}$$

The spin and momentum distributions (S18) and (S19) are shown and observed experimentally in Figs. 1 and 2 of the main text.

1.6. Example II: Interference of two standing gravity waves

As another example we consider the interference of two orthogonal standing gravity waves with equal amplitudes, or, equivalently, a superposition of four propagating waves, see Fig. 3. The complex velocity wave field for this superposition can be written as

$$W = A\left[\sin\left(kx\right) + e^{i\varphi}\sin\left(ky\right)\right],$$

$$\mathbf{V} = k^{-1}\nabla_2 W = A\left[\cos\left(kx\right)\bar{\mathbf{x}} + e^{i\varphi}\cos\left(kx\right)\bar{\mathbf{y}}\right], \tag{S20}$$

where φ is the phase between the two standing waves.

Substituting Eqs. (S20) into Eq. (S9), we obtain the spin density:

$$\mathbf{S} = \frac{\rho A^2}{\omega}\sin\varphi\cos\tilde{x}\cos\tilde{y}\,\bar{\mathbf{z}}, \tag{S21}$$

where $\tilde{x} = kx$ and $\tilde{y} = ky$. In turn, Eq. (S14) for the fields (S20) yields the canonical momentum density:

$$\mathbf{P} = \frac{\rho A^2}{2\omega}k\sin\varphi\left(\sin\tilde{x}\cos\tilde{y}\,\bar{\mathbf{y}} - \cos\tilde{x}\sin\tilde{y}\,\bar{\mathbf{x}}\right). \tag{S22}$$

The spin and momentum distributions (S21) and (S22) for $\varphi = \pi/2$ are shown and observed experimentally in Fig. 3 of the main text (see also Fig. S2 below).

2. Experimental measurements and numerical calculations

Here we describe details of experimental measurements and numerical calculations of water-particles trajectories in interference gravity-wave fields. A schematic of the experiment is shown in Fig. S1. Surface gravity waves are generated in a wave tank of size 1.0×0.6 m^2. The water depth is kept at $h = 0.1$ m to ensure the deep-water approximation for the surface waves, i.e., $\tanh(kh)\simeq 1$ [31,54], where the wavenumbers are in the range of $k = (36 - 233)\,\mathrm{m}^{-1}$ for the wave frequencies $\omega / 2\pi = (3-9)\,\mathrm{Hz}$. Sinusoidal waves are produced by two vertically oscillating paddles oriented at 90° with respect to each other, as shown in Fig. S1. The computer-controlled electrodynamic shakers (TIRA TV51140) drive the synchronised motion of two wave paddles. The paddle accelerations are measured using two accelerometers (B&K 4507) which provide feedback to the motion controllers (Vibration Research, VR9500). The phase delay φ between the paddles is adjustable in the range of $(-\pi,\pi)$ with an accuracy of ± 0.002 using a two-channel arbitrary waveform generator (HP 33120 A).

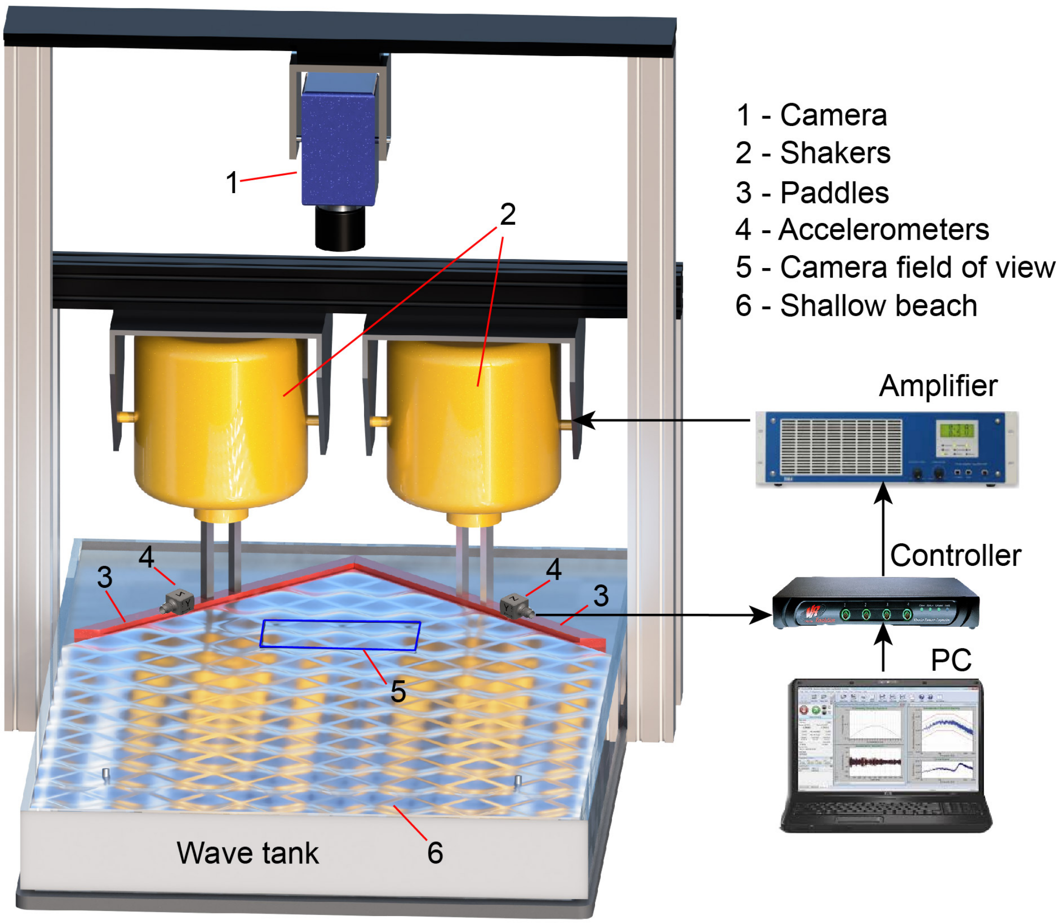

Figure S1. Schematic of the experimental setup. See explanation in the text.

In the propagating-wave configuration, a shallow beach (inclined Perspex plate) and an egg-shell absorber at the end of the wave tank are used to avoid wave reflections. In the standing-wave configuration, two wave-reflecting boundaries together with the wave paddles form a resonant square cavity of size L, which accommodates an integer number N of the wavelengths, $L = 2\pi N / k = 2\pi N g / \omega^2$.

The fluid motion at the water surface is visualised using buoyant tracer particles (Polyamid, 50 μm) illuminated by a LED panel placed underneath the transparent wave tank. A video camera (Andor Zyla X5.5; 2,560×2,160 pixel; 100 fps) with a Nikon f1.4/50 mm lens is used to capture the motion of the tracer particles. The videos are processed and analysed using the ImageJ software package.

It should be noted that the surface flows in a finite-size container can be distorted by return flows. For this reason, the tracer particle trajectories are analysed for the first ten wave periods, $t \in \left(0, 20\pi / \omega\right)$, i.e., shortly after the onset of the wave field, in order to avoid the flow distortion due to the gradual build-up of the return surface flows. Special care is also taken to avoid flows and secondary waves originating from menisci appearing along the contact lines between water, the container walls and the wave paddles. This is achieved by machining grooves on the paddles and the container boundaries at the level of the unperturbed water surface.

Figure 1B (bottom panel) of the main text shows the horizontal $\left(x, y\right)$ projection of the trajectories of the tracer particles on the water surface perturbed by the superposition of two orthogonal propagating waves of the same amplitudes and wave numbers (see Section 1.5 above). The field of view of the camera is shown in Fig. S1. The fluid particles drift in the direction of the canonical momentum (S19) and experience microscopic circular-like motion corresponding to the spin density (S18).

We compare the experimentally-measured trajectories with the numerically-computed trajectories shown in the middle panel of Fig. 1B in the main text. The numerical trajectories are computed by integrating the velocity field (S17), $\mathbf{V}\left(t, \mathbf{r}_2\right) = \mathrm{Re}\left[\mathbf{V}\left(\mathbf{r}_2\right) e^{-i\omega t}\right]$, using the 4th-order Runge-Kutta method.

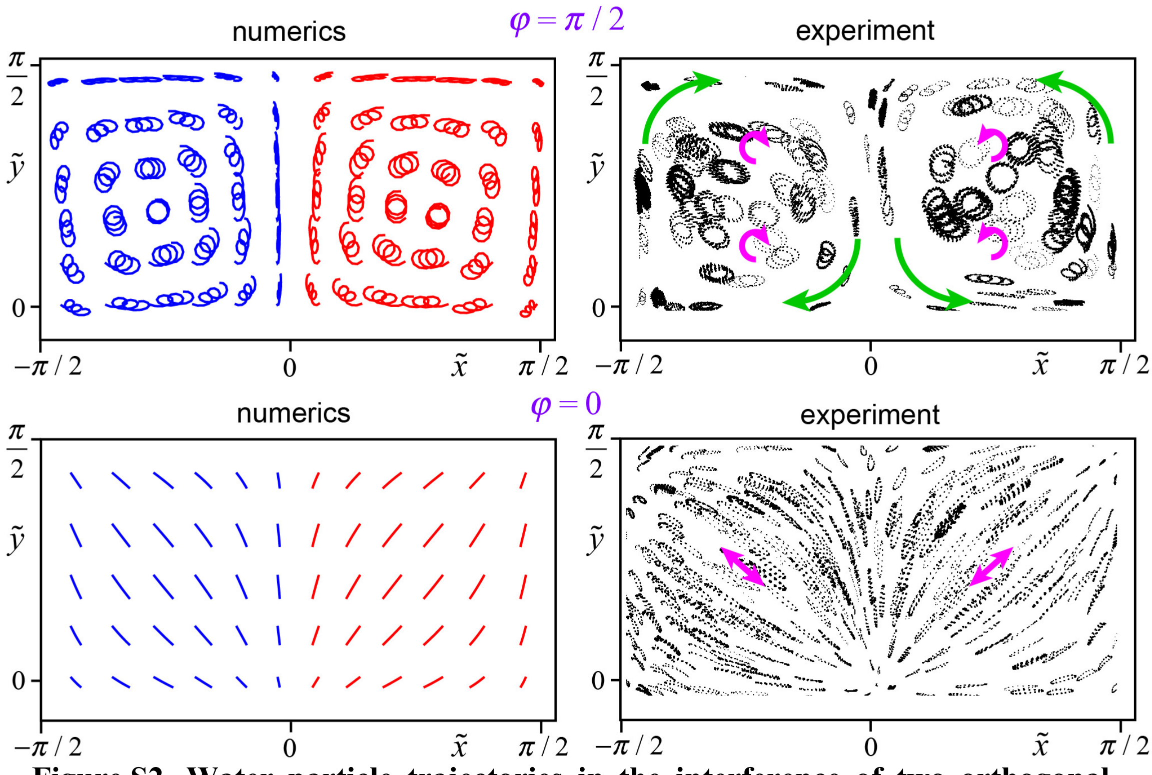

Figure S2. Water particle trajectories in the interference of two orthogonal standing gravity waves. Numerically calculated and experimentally measured trajectories are shown for two orthogonal standing waves phase-shifted by $\varphi = \pi / 2$ and $\varphi = 0$ with respect to each other (see also Fig. 3 in the main text). Here the frequency is $\omega / 2\pi = 5.3$ Hz.

For two interfering standing waves, the velocity field is given by Eq. (S20). The corresponding experimentally measured and numerically calculated trajectories are shown in Fig. 3 in the main text (for the $\varphi = \pi / 2$ case) and also in Fig. S2 (for the $\varphi = 0$ and $\varphi = \pi / 2$

cases). For $\varphi = \pi / 2$, trochoidal orbits drift around the centres of the square unit cells (with the half-wavelength π / k side), which correspond to nodal points of the surface elevation, $Z(\mathbf{r}_2, t)$. The small-scale circular motion and wavelength-scale orbital drift are in agreement with the distributions of the spin and canonical momentum, Eqs. (S21) and (S22). For $\varphi = 0$, the particles experience linear oscillations in the horizontal plane, with neither drift nor circular motion. This corresponds to the vanishing canonical momentum and spin in Eqs. (S21) and (S22): $\mathbf{P} = \mathbf{S} = \mathbf{0}$.

3. Differences between water-surface, electromagnetic, and acoustic waves

In Table I, we summarized the similarities of the spin and momentum densities involved in the Belinfante-Rosenfeld relation for electromagnetic, sound, and water waves. However, these waves are fundamentally different, both in their physical nature and mathematical properties. Here we briefly describe these differences.

First, electromagnetic waves are indeed relativistic and are described by relativistic field theory [6]. The equations of motion are Maxwell's equation:

$$\varepsilon \partial_t \mathbf{E} = \nabla \times \mathbf{H}, \qquad \mu \partial_t \mathbf{H} = -\nabla \times \mathbf{E}, \qquad \nabla \cdot \mathbf{E} = \nabla \cdot \mathbf{H} = 0, \tag{S23}$$

which describe transverse waves propagating with velocity $c = 1 \big/ \sqrt{\varepsilon \mu}$. (Note that here we use real time-dependent electric and magnetic fields, not restricted by the monochromaticity.) The linear dispersion relation of electromagnetic waves, $\omega = ck$, reflects the Minkowski spacetime structure in the problem. Equations (S23) can be derived within the Lagrangian field-theory formalism, e.g., using the Lagrangian density $\mathcal{L} = \frac{1}{2}\left(\varepsilon \mathbf{E}^2 - \mu \mathbf{H}^2\right)$ expressed via the corresponding potentials. Standard conservation laws associated with the Poincaré symmetries of the Minkowski spacetime follow from Noether's theorem applied to the above Lagrangian [6]. The first of these, the energy conservation, is the well-known Poynting theorem which is also readily derived from Maxwell's equations (S23):

$$\partial_t U + \nabla \cdot \left(c^2 \mathbf{\Pi}\right) \equiv \partial_t \left(\frac{\varepsilon \mathbf{E}^2 + \mu \mathbf{H}^2}{2}\right) + \nabla \cdot \left(\mathbf{E} \times \mathbf{H}\right) = 0. \tag{S24}$$

Here the energy density U and the energy flux density related to the kinetic momentum, $c^2 \mathbf{\Pi}$, are expressed via real time-dependent fields; their monochromatic versions in Table I are obtained by the substitution $\{\mathbf{E}, \mathbf{H}\} = \mathrm{Re}\left[\{\mathbf{E}, \mathbf{H}\} e^{-i\omega t}\right]$ and subsequent time averaging. Other Noether's conservation laws involve canonical momentum and spin densities, as described in [6,19]. An important peculiarity is that the electromagnetic Lagrangian and canonical spin/momentum densities are not uniquely defined: there are different choices for the Lagrangian density (and for the field representation via potentials) which result in the *same* equations of motion but *different* canonical spin/momentum densities [6,19,28]. Moreover, there is no microscopic theory for electromagnetism, i.e., there is no ether, and it is impossible to single out one particular choice using another, microscopic, level of description. The choice given in Table I is based on a rather abstract idea of preserving the dual symmetry between the electric and magnetic quantities [18,19,28,29].

Second, sound waves in a homogeneous fluid or gas are described by the equations [31]:

$$\beta \partial_t p = -\nabla \cdot \mathbf{v}, \qquad \rho \partial_t \mathbf{v} = -\nabla p, \qquad \nabla \times \mathbf{v} = \mathbf{0}. \tag{S25}$$

Their solutions are longitudinal waves propagating with velocity $c_s = 1 \big/ \sqrt{\beta \rho}$. Although this system is not relativistic and is considered in a single reference frame where the medium is at rest, the linear dispersion of sound waves, $\omega = c_s k$, and the equations of motion (S25) are consistent with an effective Minkowski spacetime based on the speed of sound c_s. Therefore, akin to Maxwell's equations, Eqs. (S25) can be derived within a Lagrangian field-theory formalism, e.g., using the Lagrangian density $\mathcal{L} = \frac{1}{2}\left(\rho \mathbf{v}^2 - \beta p^2\right)$ expressed via the corresponding potentials [28]. Furthermore the effective spacetime symmetry of this problem allows one to derive all the Noether conservation laws, similar to the electromagnetic ones. In particular, the energy conservation is readily obtained from Eqs. (S25) [31]:

$$\partial_t U + \nabla \cdot \left(c_s^2 \mathbf{\Pi}\right) \equiv \partial_t \left(\frac{\beta p^2 + \rho \mathbf{v}^2}{2} \right) + \nabla \cdot \left(p \mathbf{v}\right) = 0 . \tag{S26}$$

Other Noether's conservation laws involve canonical momentum and spin densities, as described in [28]. Akin to the electromagnetic case, acoustic field theory also allows different Lagrangian representations resulting in different canonical spin/momentum densities [28]. However, in contrast to electromagnetism, sound waves can also be associated with *microscopic* properties of the medium, i.e., with the motion of its molecules or atoms. This allows one to single out a specific representation consistent with the mechanical properties of this motion. In terms of Ref. [28], this is a vector-potential representation resulting in the canonical densities listed in Table I.

Finally, water-surface waves are nothing like electromagnetic or sound ones. Obviously, the system is nonrelativistic. Moreover, in contrast to the homogeneous isotropic acoustic medium, the medium is strongly inhomogeneous (with surface $z = 0$) and anisotropic (selecting the direction of the gravity force). Furthermore, the water-wave equations look nothing like Maxwell's or acoustic equations [31]. These are derived essentially using boundary conditions at the water surface. Nonetheless, in the deep-water approximation we were able to re-write water-wave equations in a form somewhat resembling acoustic equations (S25) (see Section 1 above):

$$\partial_t^2 \mathbf{V} = -g \nabla_2 W , \qquad \partial_t^2 W = g \nabla_2 \cdot \mathbf{V} , \qquad \nabla_2 \times \mathbf{V} = \mathbf{0} . \tag{S27}$$

This form is essentially based on the 2D consideration of waves and involves velocity fields at the $z = 0$ surface. It might seem that this 2D consideration would allow one to use a field-theory formalism based on (2+1) spacetime. Indeed, unperturbed water has 2D translational and rotational symmetries in the (x, y)-plane, as well as time-translation symmetry. However, the relativistic field-theory approach is fundamentally inconsistent with water-surface waves. This can be seen from the fact that water waves are inherently dispersive, $\omega = \sqrt{gk}$, which is inconsistent with the Minkowski spacetime structure requiring $\omega = ck$. (In general, the construction of relativistic field theories for dispersive waves is an open frontier problem with possible implications in quantum gravity [57].)

Another way to see that no simple Lagrangian field theory exists for Eqs. (S27) is to notice that these equations do *not* possess a simple energy conservation law similar to Eqs. (S24) and (S26). This might seem surprising: general physical considerations imply that there is no dissipation in an ideal fluid, the system is time-translation-invariant, and the energy must be conserved. In fact, there is no contradiction in the above statements. There is indeed energy conservation for water waves, but this conservation law essentially involves 3D volume fields distributed deep into water, $z < 0$ [46]. This conservation law cannot be reduced to a 2D form for the $z = 0$ fields (S27). Indeed, a generic non-monochromatic water-wave field consists of many plane waves with different wavenumbers, which therefore decay deep into the water with different exponential decay factors. As a result, the z-distribution of a generic wavefield becomes highly nontrivial. That is why the conserved energy and momentum quantities found in [46] essentially involve z-integrals. Only in the monochromatic-field case, all fields decay with the same exponent, $\propto \exp(kz)$, and the problem can be reduced to the surface field values. In this case, the energy density found in [46] yields the energy density U listed in Table I (Supplementary Materials). One can see that it has a nontrivial form different from acoustic or electromagnetic energy densities. Nonetheless, this form is physically consistent: one can check that the ratio of the momentum and energy densities in a single plane wave is consistent with the phase velocity of the wave. Namely: $\mathbf{\Pi}/U = \mathbf{P}/U = \mathbf{k}/\omega$ for all types of waves: electromagnetic, acoustic, and water-surface ones.

Thus, water waves cannot be described by an effective relativistic Lagrangian field theory, like electromagnetic and sound waves. Still, these waves possess energy and momentum conservation laws associated with the translational invariance of the system in t and (x, y) [46]. In the generic case, these conservation laws essentially involve z-integrals and fields in volume, but for monochromatic waves the conserved densities are reduced to the surface values U and $\mathbf{\Pi}$ listed in Table I. Despite the absence of an effective Lagrangian field theory, one can derive the momentum and intrinsic angular momentum (spin) densities from the *microscopic* consideration of water particles. Akin to the sound-wave theory, this yields the canonical momentum $\mathbf{P}$ and spin $\mathbf{S}$ listed in Table I. Most remarkably, the conserved kinetic momentum $\mathbf{\Pi}$ and canonical quantities $\mathbf{P}$ and $\mathbf{S}$ precisely satisfy the Belinfante-Rosenfeld relation (1). This suggests that the Belinfante-Rosenfeld construction can have a deeper origin than a standard relativistic field theory.

It is natural to expect that the z-component of the angular momentum is also conserved in the rotationally invariant system under consideration. Then, the relations between the conserved (x, y)-momentum and z-directed angular momentum should be described by the standard Belinfante-Rosenfeld relations. Namely, the kinetic angular momentum density is given by $(\mathbf{r}_2 \times \mathbf{\Pi})$, $\mathbf{r}_2 \equiv (x, y)$, while the canonical angular momentum consists of the orbital and spin parts: $(\mathbf{r}_2 \times \mathbf{P}) + \mathbf{S}$. The integrals of these densities coincide with each other for a localized field. In contrast to earlier, rather sophisticated field-theory descriptions of water waves [32–35], our work put forward and verifies experimentally intuitively clear, directly observable momentum and angular momentum properties of surface gravity waves.

To summarize this comparison, the Belinfante-Rosenfeld relation is the only fundamental and nontrivial similarity in the description of water-wave and electromagnetic or acoustic fields. The other equations and properties differ profoundly.

REFERENCES AND NOTES

1. G. E. Uhlenbeck, S. Goudsmit, Spinning electrons and the structure of spectra. *Nature* **117**, 264–265 (1926).

2. Spin, *Nature Milestones* S5–S20 (2008); https://www.nature.com/collections/idgejiafca/#:text=The%20Milestones%20arre%20a%20series,reviews%20from%20Nature%20Publishing%20Group.

3. V. B. Berestetskii, E. M. Lifshitz, L. P. Pitaevskii, *Quantum Electrodynamics* (1982).

4. F. J. Belinfante, On the current and the density of the electric charge, the energy, the linear momentum and the angular momentum of arbitrary fields. *Physica* **7**, 449–474 (1940).

5. L. Rosenfeld, On the energy-momentum tensor. *Memoirs Acad. Roy. de Belgique* **18**, 1–30 (1940).

6. D. E. Soper, *Classical Field Theory* (Wiley, 1976).

7. H. C. Ohanian, What is spin? *Am. J. Phys.* **54**, 500–505 (1986).

8. S. A. Wolf, D. D. Awschalom, R. A. Buhrman, J. M. Daughton, S. von Molnar, M. L. Roukes, A. Y. Chtchelkanova, D. M. Treger, Spintronics: A spin-based electronics vision for the future. *Science* **294**, 1488–1495 (2001).

9. I. Zutic, J. Fabian, S. Das Sarma, Spintronics: Fundamentals and applications. *Rev. Mod. Phys.* **76**, 323–410 (2004).

10. I. Buluta, S. Ashhab, F. Nori, Natural and artificial atoms for quantum computation. *Rep. Prog. Phys.* **74**, 104401 (2011).

11. J. J. Pla, K. Y. Tan, J. P. Dehollain, W. H. Lim, J. J. L. Morton, D. N. Jamieson, A. S. Dzurak, A. Morello, A single-atom electron spin qubit in silicon. *Nature* **489**, 541–545 (2012).

12. L. M. K. Vandersypen, H. Bluhm, J. S. Clarke, A. S. Dzurak, R. Ishihara, A. Morello, D. J. Reilly, L. R. Schreiber, M. Veldhorst, Interfacing spin qubits in quantum dots and donors–hot, dense, and coherent. *npj Quantum Inf.* **3**, 34 (2017).

13. J. H. Poynting, The wave-motion of a revolving shaft, and a suggestion as to the angular momentum in a beam of circularly-polarized light. *Proc. R. Soc. Lond. A* **82**, 560–567 (1909).

14. R. A. Beth, Mechanical detection and measurement of the angular momentum of light. *Phys. Rev.* **50**, 115–125 (1936).

15. N. B. Simpson, K. Dholakia, L. Allen, M. J. Padgett, Mechanical equivalence of spin and orbital angular momentum of light: An optical spanner. *Opt. Lett.* **22**, 52–54 (1997).

16. *The Angular Momentum of Light*, D. L. Andrews, M. Babiker, Eds. (Cambridge Univ. Press, 2013).

17. K. Y. Bliokh, F. Nori, Transverse and longitudinal angular momenta of light. *Phys. Rep.* **592**, 1–38 (2015).

18. R. P. Cameron, S. M. Barnett, A. M. Yao, Optical helicity, optical spin and related quantities in electromagnetic theory. *New J. Phys.* **14**, 053050 (2012).

19. K. Y. Bliokh, A. Y. Bekshaev, F. Nori, Dual electromagnetism: Helicity, spin, momentum and angular momentum. *New J. Phys.* **15**, 033026 (2013).

20. K. Y. Bliokh, F. J. Rodríguez-Fortuño, F. Nori, A. V. Zayats, Spin-orbit interactions of light. *Nat. Photonics* **9**, 796–808 (2015).

21. A. Aiello, P. Banzer, M. Neugebauer, G. Leuchs, From transverse angular momentum to photonic wheels. *Nat. Photonics* **9**, 789–795 (2015).

22. P. Lodahl, S. Mahmoodian, S. Stobbe, A. Rauschenbeutel, P. Schneeweiss, J. Volz, H. Pichler, P. Zoller, Chiral quantum optics. *Nature* **541**, 473–480 (2017).

23. W. L. Jones, Asymmetric wave-stress tensors and wave spin. *J. Fluid Mech.* **58**, 737–747 (1973).

24. Y. Long, J. Ren, H. Chen, Intrinsic spin of elastic waves. *Proc. Natl. Acad. Sci. U.S.A.* **115**, 9951–9955 (2018).

25. C. Shi, R. Zhao, Y. Long, S. Yang, Y. Wang, H. Chen, J. Ren, X. Zhang, Observation of acoustic spin. *Natl. Sci. Rev.* **6**, 707–712 (2019).

26. K. Y. Bliokh, F. Nori, Spin and orbital angular momenta of acoustic beams. *Phys. Rev. B* **99**, 174310 (2019).

27. I. D. Toftul, K. Y. Bliokh, M. I. Petrov, F. Nori, Acoustic radiation force and torque on small particles as measures of the canonical momentum and spin densities. *Phys. Rev. Lett.* **123**, 183901 (2019).

28. L. Burns, K. Y. Bliokh, F. Nori, J. Dressel, Acoustic versus electromagnetic field theory: Scalar, vector, spinor representations and the emergence of acoustic spin. *New J. Phys.* **22**, 053050 (2020).

29. M. V. Berry, Optical currents. *J. Opt.* **11**, 094001 (2009).

30. K. Y. Bliokh, A. Y. Bekshaev, F. Nori, Extraordinary momentum and spin in evanescent waves. *Nat. Commun.* **5**, 3300 (2014).

31. L. D. Landau, E. M. Lifshitz, *Fluid Mechanics* (Butterworth-Heinemann, 1987).

32. R. L. Seliger, G. B. Whitham, Variational principles in continuum mechanics. *Proc. R. Soc. Lond. A* **305**, 1–25 (1968).

33. L. J. F. Broer, On the Hamiltonian theory of surface waves. *Appl. Sci. Res.* **30**, 430–446 (1974).

34. T. Brooke Benjamin, P. J. Olver, Hamiltonian structure, symmetries and conservation laws for water waves. *J. Fluid Mech.* **125**, 137–185 (1982).

35. T. G. Shepherd, Symmetries, conservation laws, and Hamiltonian structure in geophysical fluid dynamics. *Adv. Geophys.* **32**, 287–338 (1990).

36. G. G. Stokes, On the theory of oscillatory waves. *Trans. Cambridge Philos. Soc.* **8**, 441–455 (1847). Reprinted in G.G. Stokes, Mathematical and Physical Papers, vol. 1 (Cambridge Univ. Press, 1880).

37. M. S. Longuet-Higgins, Mass transport in water waves. *Philos. Trans. R. Soc. A* **245**, 535–581 (1953).

38. T. S. van den Bremer, Ø. Breivik, Stokes drift. *Philos. Trans. R. Soc. A* **376**, 20170104 (2017).

39. M. V. Berry, M. R. Dennis, Polarization singularities in isotropic random vector waves. *Proc. R. Soc. Lond. A* **457**, 141–155 (2001).

40. N. Riley, Acoustic streaming. *Theor. Comput. Fluid Dyn.* **10**, 349–356 (1998).

41. J. Friend, L. Y. Yeo, Microscale acoustofluidics: Microfluidics driven via acoustics and ultrasonics. *Rev. Mod. Phys.* **83**, 647–704 (2011).

42. W. Connacher, N. Zhang, A. Huang, J. Mei, S. Zhang, T. Gopesh, J. Friend, Micro/nano acoustofluidics: Materials, phenomena, design, devices, and applications. *Lab Chip* **18**, 1952–1996 (2018).

43. D. G. Andrews, M. E. McIntyre, On wave-action and its relatives. *J. Fluid Mech.* **89**, 647–664 (1978).

44. M. S. Longuet-Higgins, Spin and angular momentum in gravity waves. *J. Fluid Mech.* **97**, 1–25 (1980).

45. M. Kubota, A mechanism for the accumulation of floating marine debris north of Hawaii. *J. Phys. Oceanogr.* **24**, 1059–1064 (1994).

46. C. S. Peskin, Wave momentum (The Silver Dialogues, New York Univ., 2010); www.math.nyu.edu/faculty/peskin/papers/wave_momentum.pdf.

47. A. Y. Bekshaev, K. Y. Bliokh, F. Nori, Transverse spin and momentum in two-wave interference. *Phys. Rev. X* **5**, 011039 (2015).

48. N. Francois, H. Xia, H. Punzmann, P. W. Fontana, M. Shats, Wave-based liquid-interface metamaterials. *Nat. Commun.* **8**, 14325 (2017).

49. J. Sinova, S. O. Valenzuela, J. Wunderlich, C. H. Back, T. Jungwirth, Spin Hall effects. *Rev. Mod. Phys.* **87**, 1213–1260 (2015).

50. R. Takahashi, M. Matsuo, M. Ono, K. Harii, H. Chudo, S. Okayasu, J. Ieda, S. Takahashi, S. Maekawa, E. Saitoh, Spin hydrodynamic generation. *Nat. Phys.* **12**, 52–56 (2016).

51. M. E. McIntyre, On the “wave momentum” myth. *J. Fluid Mech.* **106**, 331–347 (1981).

52. M. Stone, Phonons and forces: Momentum versus pseudomomentum in moving fluids, in *Artificial Black Holes*, M. Novello, M. Visser, G. Volovik, Eds. (World Scientific, 2002).

53. D. G. Grier, A revolution in optical manipulation. *Nature* **424**, 810–816 (2003).

54. J. Lighthill, *Waves in Fluids* (Cambridge Univ. Press, 2001).

55. K. Y. Bliokh, D. Smirnova, F. Nori, Quantum spin Hall effect of light. *Science* **348**, 1448–1451 (2015).

56. K. Y. Bliokh, F. Nori, Transverse spin and surface waves in acoustic metamaterials. *Phys. Rev. B* **99**, 020310(R) (2019).

57. M. Visser, Emergent rainbow spacetimes: Two pedagogical examples; arXiv:0712.0810 (2007).